On the Precipitation Sequence in a 10%Cr Steel under Tempering

Nadezhda DUDOVA and Rustam KAIBYSHEV

Belgorod State University, Pobeda 85, Belgorod, 308015 Russia.

Precipitation sequence under tempering in a 10%Cr steel has been considered in details. Two different precipitation processes have been identified, concurrently. First, at 350°C, a dispersion of M_2C phase with orthorhombic lattice appears. At 525°C, the M_2C phase is displaced by the formation of $M_{23}C_6$ carbide. However, this process remains uncompleted. Dissolution of M_2C phase occurs completely due to the formation and growth of more stable M_6C phase as a result of tempering in the range of 650 to 770°C. Second, Nb-rich and V-rich M(C,N) carbonitrides precipitate in the temperature interval of 500–770°C. These dispersoids play a role of heterogeneous nucleation sites for precipitations of $M_{23}C_6$ and M_6C carbides.

KEY WORDS: high chromium martensitic steel; precipitation behavior; tempering.

1. Introduction

Recently high-chromium steels with tempered martensite lath structure (TMLS) became widely used as materials for fossil power plants.[1,2] The ability of these steels to be creep resistant depends critically on the carbide distribution in their microstructure that is dictated by a tempering treatment, mainly.[3,4] Nature and origin, size and distribution of these secondary phases control creep behavior and, therefore, determine exploitation temperature of martensitic steels.[2–9]

These martensitic steels are commonly used in a "normalized and tempered" condition.[1–11] This heat treatment involves austenitizing that dissolves the carbides, followed by an air cooling that transforms the austenite to martensite. Finally, these steels are subjected to tempering to produce TMLS stabilized by nanoscale carbides. Precipitation behavior during heat treatment of 9% chromium steels was examined in several works.[7–15] The decomposition of martensite that provides the precipitation of secondary phases is characterized by two reactions taking place concurrently. The first reaction results in the formation of MX carbonitrides distinctly separated into Nb-rich M(C,N) and V-rich M(C,N) particles.[7] Two-phase separation of MX carbonitrides being thermodynamically equilibrium is extremely important for achieving high creep resistance.[4,6,9,16] Namely, the co-existence of Nb-rich M(C,N) and V-rich M(C,N) carbonitrides prevents coarsening of these dispersoids under creep conditions. It seems that a ratio between Nb-rich M(C,N) and V-rich M(C,N) carbonitrides appeared after tempering strongly affects the creep behavior of the martensitic steels. It is worth noting that relatively coarse particles of Nb-rich M(C,N) are observed within martensitic matrix after normalization,[9,17] which may remain undissolved during austenitizing treatment or may precipitate from austenite during air quenching.[9,18]

The second reaction results in the formation of $M_{23}C_6$ carbides on the boundaries of prior austenite grains, packets, blocks and laths.[9–15,19] Two sequences of carbide precipitation were found. First sequence was reported[10,12] as follows:

$$\text{martensite} \rightarrow M_3C \rightarrow M_2C \rightarrow M_{23}C_6 \quad \text{..... (1)}$$

It should be noted that the M_2C was identified as Cr_2N phase with hexagonal lattice (a=0.28 nm and c=0.445 nm).[10,12] The other sequence was reported in[9,11,20] as follows:

$$\text{martensite} \rightarrow M_3C \rightarrow M_7C_3 \rightarrow M_{23}C_6 \quad \text{..... (2)}$$

This sequence was recently found for a 3%Co modified P911-type steel.[18] Creep resistance of martensitic steels can be significantly enhanced by refinement of $M_{23}C_6$ carbides and increase in their coarsening resistance. This goal is achieved by additional alloying with boron.[20]

It was shown[13,21] that boron strongly affects the tempering processes in high chromium steel, decreasing the size of $M_{23}C_6$ carbides and increasing their coarsening resistance due to the formation of $M_7(B{\cdot}C)_3$ and $M_{23}(B{\cdot}C)_6$ phase in the precipitation sequence (2) instead of M_7C_3 and $M_{23}C_6$ carbides, respectively. Equilibrium boron segregation on high-angle boundaries provides extensive refinement of $M_{23}(B{\cdot}C)_6$ located on these boundaries,[13] while the small carbides located within interiors of block are almost free of boron.[13,20–23] Boron additions suppress the coarsening of $M_{23}C_6$ on the grain boundaries during creep, thus, improving the creep strength. The formation of boron enriched M_6C was found in a steel containing 100 ppm of B.[24] It seems that boron additives modify the precipitation sequence (2) as follows[25]

$$\text{martensite} \rightarrow M_3C \rightarrow M_7C_3 \rightarrow M_{23}C_6 \rightarrow M_6C \quad \text{..... (3)}$$

Thus, the precipitation sequence in high chromium steels strongly depends on their chemical composition. Exact understanding of precipitation mechanisms during heat treatment is important. In the present work the precipitation sequence is analyzed in a 10%Cr steel containing 80 ppm of B.

This steel was developed for use in trial rotor and blades for advanced steam conditions by Toshiba and refers as TOS110.[1)] However, there is a little published data on structure and mechanical properties of this steel. This steel is distinctly different from the other martensitic steels for fossil power plants by boron and cobalt additives and increased chromium content. Thus, the aim of the present work is to examine the precipitation behavior of the 10%Cr steel as a function of tempering conditions. An understanding of precipitation sequence allows an interpretation of tempering effect on structure and mechanical properties of this steel.

2. Experimental

The steel studied was (in mass%) 0.1%C; 0.06%Si; 0.1%Mn; 10.0%Cr; 0.17%Ni; 0.7%Mo; 0.05%Nb; 0.2%V; 0.003%N; 0.008%B; 2.0%W; 3.0%Co; 0.01%Ti; 0.006%Cu; 0.01%Al and Fe-balance. This material is denoted as the 10%Cr steel, herein. 500 kg steel ingot was prepared by vacuum induction melting. Next, the steel was homogenized at 1 160°C and subsequently forged into a strip with a cross-section size of 65 mm × 140 mm with a finish-forging temperature of 850°C. The samples for structural characterization were machined from the strip, which finally was normalized at 1 060°C for 30 min, air cooled and tempered at temperature of 300–800°C for 3 h.

After the heat treatment the steel was examined by an Olympus GX70 optical microscope, a JEM-2100 transmission electron microscope (TEM) operated at 200 kV that was equipped with an INCA energy-dispersive X-ray spectrometer (EDS) and a Quanta 200 scanning electron microscope. For TEM examinations, samples were cut and thinned to about 0.1 mm. Discs with a 3 mm diameter were electropolished to perforation with a Tenupol-5 twinjet polishing unit using a 10% solution of perchloric acid in glacial acetic acid. In addition extraction replicas on copper grids were used for precipitate analysis in order to avoid matrix effects when obtaining EDS spectra. The specimens were mechanically polished by emery paper and 3 μm silica suspension, and then etched using a solution of 3 mL hydrochloric acid and 1 g picric acid in 10 mL of ethanol. The size distribution and mean radius of the secondary phase particles were evaluated by taking of 15 TEM micrographs, corresponding to 150–250 particles per a specimen. The precipitates were identified by chemical composition and diffraction pattern.

Differential scanning calorimetry (DSC) was performed on a ~45 mg specimen during heating to 1 100°C at a rate of 20°C min^{-1} and cooling in argon atmosphere with the same rate by using an SDT Q600 (TA Instruments) calorimeter. The dilatometric measurements were carried out using a NETZSCH model DIL 402C dilatometer with rod-shaped samples with a length of 25 mm and a diameter of 6 mm. Equilibrium mole fractions of phases and their chemical composition were calculated with a version 5 of the Thermo-Calc software using the TCFE6 database.

3. Experimental Results

3.1. Thermodynamic Calculations

Thermo-Calc calculations were carried out for the steel with a composition of 0.1%C; 0.1%Si; 0.08%Mn; 10.0%Cr; 0.2%Ni; 0.7%Mo; 0.05%Nb; 0.2%V; 0.003%N; 0.01%B; 2.0%W; 3.0%Co; 0.01%Ti; 0.003%Al; 0.01%P; 0.01%Cu; Fe-balance to determine the influence of main alloying elements on the phase composition at different temperatures. Results of Thermo-Calc calculations at austenization temperature of 1 060°C, and at different tempering temperatures (350, 525, 650, 750 and 770°C) are shown in **Fig. 1**. At 1 060°C, a small amount (mole fraction less than 0.001) of un-dissolved NbC was predicted (Fig. 1(a)). Following phases were predicted by Thermo-Calc calculations: presence of Laves phase at temperatures ranging from 350 to 750°C; $M_{23}C_6$ carbides enriched by Cr and Mo at low temperatures (350–525°C). It is worth noting that Σ(Mo+W)~20 mass% was predicted in $M_{23}C_6$ carbide being essentially independent on temperature, while Mo and W contents tend to decrease and increase, respectively, with increasing temperature (Fig. 1(b)). At all tempering temperatures, the presence of NbC and TiN was predicted.

3.2. Normalized Conditions

The microstructure produced by air cooling is shown in **Fig. 2**. An average size of prior austenite grains (PAG) is about 35 μm. A small amount (2%) of δ-ferrite was revealed by optical metallography (Fig. 2(a)). Average thickness of martensite laths is about 0.2 μm. TEM revealed a dispersion of needle-like Fe-rich M_3C particles with an average length of about 60 nm within martensitic laths (Fig. 2(b)). M_3C particles obey the following orientation relationship to the ferritic matrix: $(001)_{M3C} \,||\, (011)_{\alpha\text{-Fe}}$. It seems that these dis-

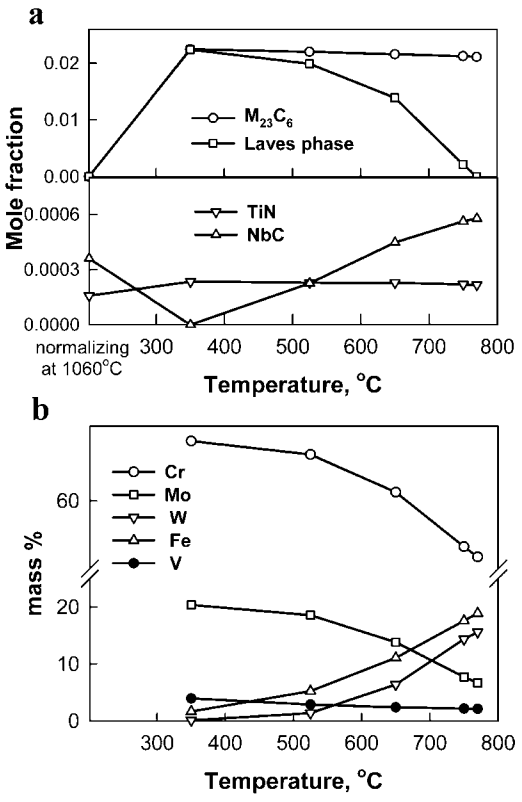

Fig. 1. (a) Equilibrium mole fraction of phases at different temperatures calculated by Thermo-Calc. (b) Quantitative values of elements in $M_{23}C_6$ carbides at different temperatures calculated by Thermo-Calc.

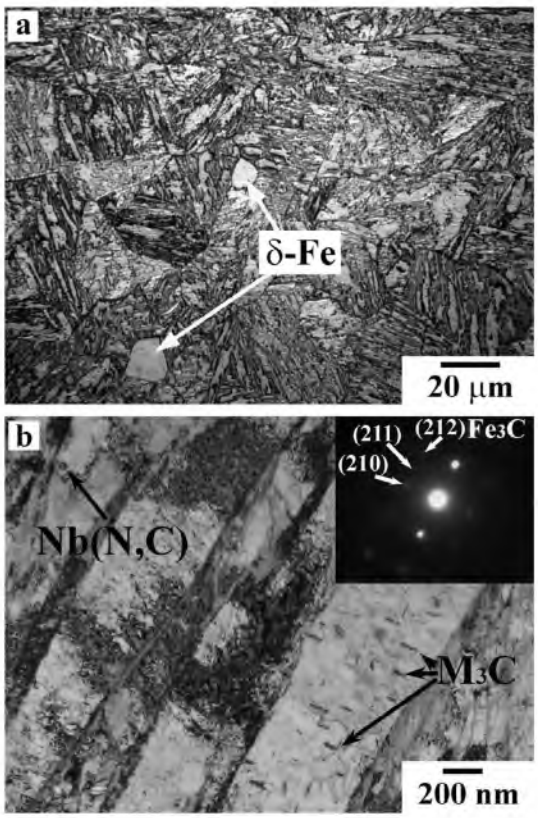

Fig. 2. The microstructure of steel after normalizing at 1 060°C: (a) optical microscopy, (b) TEM micrograph shows different precipitations and electron diffraction pattern from M_3C.

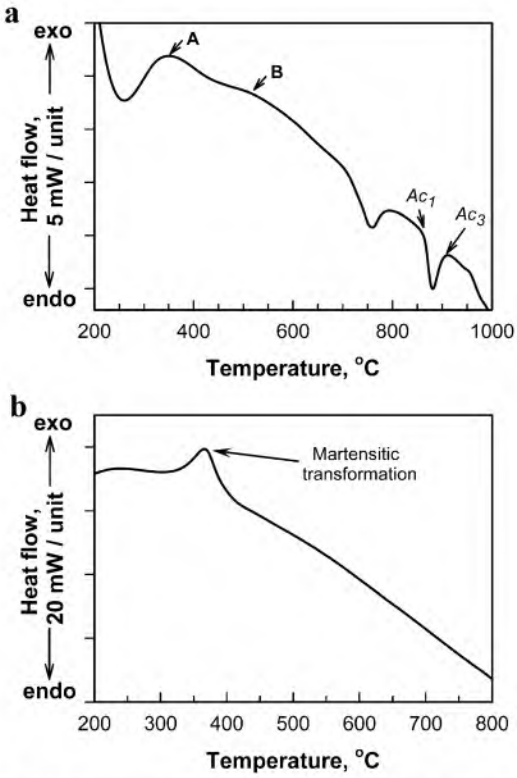

Fig. 3. DSC curves obtained during heating (a) and cooling (b) at rate of 20°C/min after normalizing at 1 060°C.

persoids have precipitated from austenite during air cooling.[9] Volume fraction of Nb(N,C) particles with an average size of about 170 nm is negligible (about 0.02%) (Fig. 2(b)). These coarse particles seem to remain undissolved under normalization conditions.

Figure 3 shows DSC curves obtained on heating and cooling conditions of the steel subjected to normalization treatment from 1 060°C. Two exothermic peaks of A and B attributed to precipitations were found at 350 and 520°C (Fig. 3(a)). A_{c1} temperature for the 10%Cr steel is about 865°C. Prior to the A_{c1} transformation, the endothermic peak was observed during heating with a peak temperature of 755°C. This is a result of a magnetic transition from a ferromagnetic state to a paramagnetic state. The curve during cooling showed the exothermic peak resulting from the martensitic transformation below 400°C (Fig. 3(b)). The martensitic transformation temperatures were clarified by means of dilatometric analysis, which showed that for cooling rate of 2°C/min the martensitic transformation occurred in the temperature range of 398–348°C.

3.3. Tempered Conditions

Figure 4 shows TEM micrographs of the steel tempered for 3 h at different temperatures. At 350°C, the formation of two types of dispersoids was detected. First, dispersoids having equiaxed shape with an average size of about 20 nm were found within the martensite laths. These particles were identified as NbC carbides (Fig. 4(a)). The EDX data revealed that most of these particles contain mainly Nb (**Fig. 5**(a)); traces of V (about 3 mass%) and Ti (about 1.5 mass%)

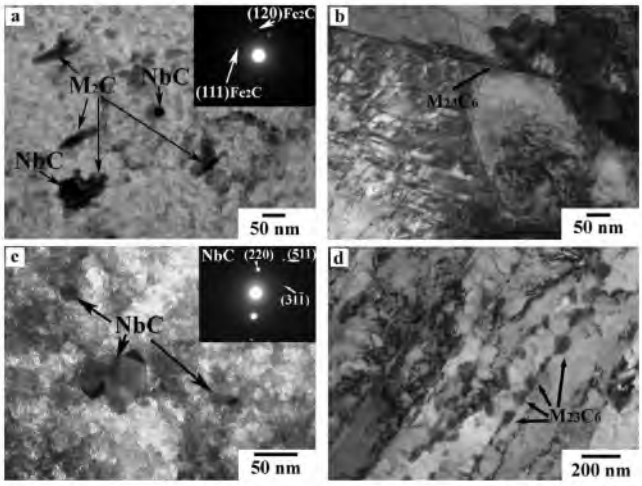

Fig. 4. TEM micrographs of normalized-and-tempered steel show different precipitations and corresponding electron diffraction patterns: (a) 350°C (carbon replica), (b), (c) 525°C (c – carbon replica), (d) 650°C.

particles enriched by Cr, Fe, W and V. It is worth noting that dispersoids enriched by tungsten exhibit different contrast: edges of these dispersoids show well-defined black contrast while their core is relatively grew. We can presume that nucleation of M_2C carbides enriched by W takes place on interface boundaries of NbC/martensite. Therefore, the MX carbides are apparently enriched by W (about 45 mass%). Unfortunately, we could not unambiguously identify its lattice by diffraction. Second type of dispersoids exhibits needle-type shape and contains mainly Fe, W and Cr (Fig. 5(a)). These dispersoids were identified as M_2C carbides with orthorhombic structure (Fig. 4(a)). Their length and

thickness are about 100 and 20 nm, respectively. Crystal lattice of these particles was identified.

At 525°C, the formation of film-like $M_{23}C_6$ carbides takes place along high-angle boundaries of PAGs and packets (Fig. 4(b)). A dispersion of NbC particles with an average size of about 30 nm was observed within the martensite laths (Fig. 4(c)). These particles are enriched by W and Cr (Fig. 5(b)) as described above.

At 650°C, the formation of $M_{23}C_6$ carbides having equiaxed shape with an average size of about 50 nm occurs (Fig. 4(d)). These carbides are located on high-angle and lath boundaries. It seems that these carbides result from two processes: coagulation of film-like $M_{23}C_6$ carbide precipitated at 525°C on high-angle boundaries of PAGs and packets and independent precipitation of $M_{23}C_6$ carbides on block and lath boundaries, mainly. The second process is in dominant. At this temperature, thickness of martensite laths slightly increases to about 0.25 μm.

At 770°C, the width of martensite lath increases up to about 0.5 μm (**Fig. 6**(a)). The fraction of $M_{23}C_6$ carbides exhibiting essentially equiaxed shape is about 2%. Normal distribution with a long end part of the mean size of these particles is observed (Fig. 6(b)). Two different fractions of $M_{23}C_6$ carbides could be distinguished by location. Coarse $M_{23}C_6$ carbides locate at high-angle boundaries, and nanoscale $M_{23}C_6$ carbides locate on low-angle lath boundaries. Average size of $M_{23}C_6$ carbides located at high-angle boundaries is about 100 nm. However, size of separate $M_{23}C_6$ carbides belonging to this fraction may attain 300–400 nm (Fig. 6(b)). Average size of $M_{23}C_6$ carbides belonging to second fraction is about 60 nm. The coexistence of two fractions of $M_{23}C_6$ carbides distinguished by their size and location suggests thermodynamic instability of fine $M_{23}C_6$ carbides.[26] Under creep condition the coarse $M_{23}C_6$ carbides located on high-angle boundaries tend to grow; and fine $M_{23}C_6$ carbides located on lath boundaries dissolve.[26,27] The EDX revealed that the $M_{23}C_6$ carbides contain mainly Cr and Fe (Fig. 5(c)). In addition, the presence of such elements as Mo, W and V was also detected within these carbides. Their content is in consistent with that predicted by Thermo-Calc calculations (Fig. 1(b)). Several coarse carbides located on high-angle boundaries contain boron.[20]

The NbC particles with slightly increased size of about 50 nm exhibiting well-defined equiaxed shape were also revealed after tempering at 770°C (Fig. 6(c)). The EDX analysis showed that the content of Cr, W and Fe in the NbC particles decreases, while content of V increases to 12 mass% (Fig. 5(c)). Fine V-rich carbonitrides M(C,N) having a "wing" shape[14,28] with an average length of about 30 nm were detected (Fig. 6(d)). On the other hand, V-rich M(C,N) carbonitrides having equiaxed shape could be rarely observed. It is worth noting that Nb-rich and V-rich M(C,N) carbonitrides could be easily distinguished by their morphology.

In addition, fine W-rich particles were found (Fig. 6(c)). These dispersoids exhibit equiaxed shape and their average size is about 25 nm that is smaller than an average size of the $M_{23}C_6$ carbides by a factor of about 3. The EDX revealed that the content of W in these dispersoids reaches about 78 mass% (or 50 at%) (Fig. 5(c)). Fe and Cr were also detected. Interpretation of microdiffraction patterns taken from these

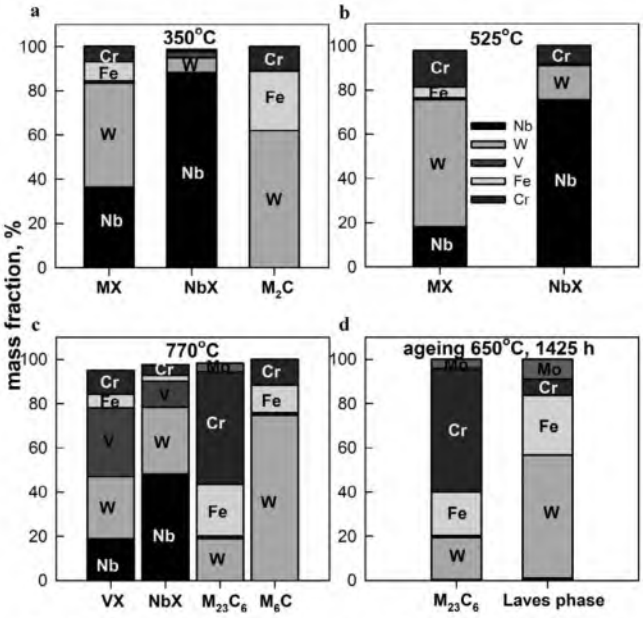

Fig. 5. Mass fraction of elements in different phases in normalized-and-tempered steel at: (a) 350°C, (b) 525°C, (c) 770°C, and (d) after ageing at 650°C for 1 425 h, measured from replicas by EDX with TEM.

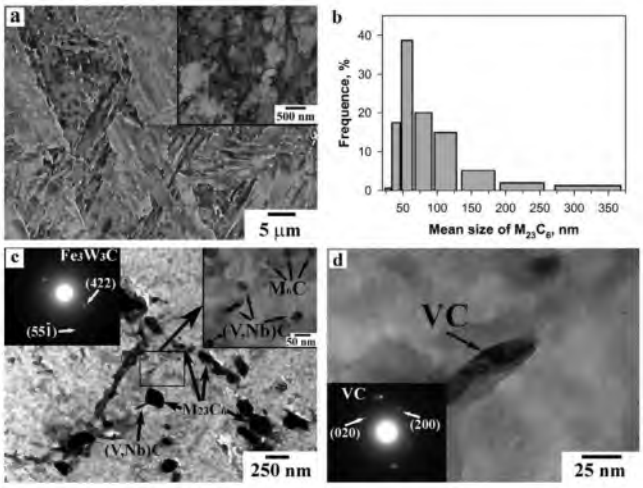

Fig. 6. Microstructures of normalized-and-tempered steel at 770°C: (a) TEM+SEM, (b) mean size of $M_{23}C_6$ distribution, (c), (d) TEM micrographs (replica) show different precipitations and corresponding electron diffraction patterns.

dispersoids (Fig. 6(c)) suggested that these particles are Fe_3W_3C carbides. Thus, the initial stage of the formation of M_6C carbides occurs under high-temperature tempering. It is seen that these carbides precipitate along lath boundaries, mainly. Therefore, precipitations of the $M_{23}C_6$ and M_6C carbides can serve to impede grain boundary mobility and thereby restrict the lath coarsening.[18,27] The M_6C carbides are most efficient in stabilization of TMLS under creep conditions to finest size.

4. Discussion

Inspection of experimental data shows that precipitation of MX carbonitrides occurs in the 10%Cr steel in the same way as in commercial 9% Cr creep resistant steels and

results in well-known two-phase separation of Nb-rich and V-rich M(C,N).[4,6,9,16] This two-phase separation provides high creep resistance of the 10%Cr steel.

In contrast, the formation of carbides in the present steel takes place in accordance with a unique sequence, which can be represented as follows

$$\text{martensite} \rightarrow M_3C \rightarrow M_2C \rightarrow M_{23}C_6 \text{ and } M_6C \ldots\ldots (4)$$

This sequence has two unusual features. First, the formation of the M_2C carbides with orthorhombic lattice follows the formation of M_3C carbide. Second, the formation of M_6C occurs concurrently with the $M_{23}C_6$ carbides at high temperatures. Thus, two–phase separation of carbides occurs. This can be favorable for creep resistance of the 10%Cr steel due to hindering the carbide coarsening. This feature is attributed to tungsten and cobalt additives to this steel.[18] It is noticeable that boron additives provide average size of $M_{23}C_6$ and M_6C carbides much less than 100 nm. Enrichment by boron of these carbides located on high-angle boundaries can provide their resistance to coarsening that is important for creep resistance. $M_{23}C_6$ carbide is equilibrium one. However, M_6C carbide may be metastable one because it is not predicted by thermodynamic calculations. In order to obtain an evidence for instability of M_6C phase, an examination of a sample subjected to long-term ageing under creep conditions was performed (**Fig. 7**).

Predicted Laves phase (Fig. 1(a)) was not observed in all specimens tempered in the temperature interval of 350–770°C, perhaps due to a short annealing time (3 h). It seems that M_6C carbides tend to coarsening and play a role of nucleation sites for the formation of Laves phase ($Fe_2(W,Mo)$) during long-term ageing (Fig. 7(a)). In the steel exposed for 1 425 h at 650°C, the particles of Laves phase with an average size of 100 nm evolved in the vicinity or even on the interface boundaries of M_6C carbides (Fig. 7(a)). The stacking faults formed within the Laves phases (No. 1 on Fig. 7(a)) are observed as characteristic streaks on the selected area electron diffraction pattern (Fig. 7(b)). These particles of Laves phase contain about 50 mass% W and about 10 mass% Mo (Fig. 5(d)). The other particles (No.2 on Fig. 7(a)) with the same chemical composition exhibit spots originated from Laves phase as well as the spots originated from M_6C on the selected area electron diffraction pattern (Fig. 7(b)). Therefore, the appearance of Laves phase could occur due to either a nucleation on interface boundaries of existing M_6C carbides, or a transformation of M_6C carbides into Laves phase by W and Mo diffusion from the steel matrix into a M_6C particle resulting in transformation of cubic lattice into hexagonal one. Thus, M_6C carbides is a metastable phase in the present 10%Cr steel which can be replaced by Laves phase during long-term ageing under creep conditions. Therefore, average size of $M_{23}C_6$ and M_6C carbides can be decreased by boron and tungsten additives under tempering. However, only boron provides coarsening resistance of $M_{23}C_6$ carbides under creep conditions.

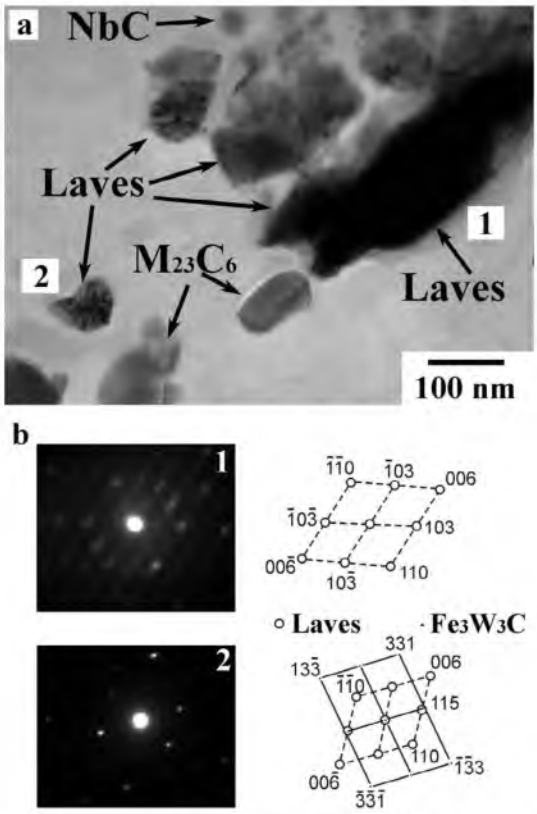

Fig. 7. Laves phases formed during ageing at 650°C for 1 425 h: (a) TEM micrograph (replica) and (b) corresponding electron diffraction patterns from particles No. 1 and No. 2.

5. Summary

The precipitation behavior of the 10%Cr steel as a function of tempering conditions (300–800°C for 3 h) can be summarized as follows:

(1) In the normalized from 1 060°C condition the M_3C and negligible amount of Nb(N,C) precipitations are formed.

(2) The precipitation sequence of $M_3C \rightarrow M_2C \rightarrow (M_{23}C_6$ and $M_6C)$ is observed in the 10%Cr steel under tempering.

(3) The formation of transient M_2C carbide and MX carbonitride occurs at 350°C. At T≥525°C, $M_{23}C_6$ carbides are formed. Increasing temperature to 770°C results in the formation of M_6C carbides. These carbides are metastable ones and are replaced by Laves phase under long-term ageing.

(4) At 770°C, tempering results in the two-phase separation of MX carbonitrides into Nb-rich and V-rich particles.

Acknowledgements

The financial support received from the Federal Agency for Science and Innovations, Russia, under grant no. P1095 is gratefully acknowledged. The authors are grateful to the personnel of the Joint Research Centre, Belgorod State University, for their assistance with instrumental analysis.

REFERENCES

1) R. Viswanathan, J. F. Henry, J. Tanzosh, G. Stanko, J. Shingledecker, B. Vitali and R. Purgert: *J. Mater. Eng. Perfor.*, **14** (2005), 281.
2) R. O. Kaibyshev, V. N. Skorobogatykh and I. A. Shchenkova: *The Phys. Met. Metallography*, **109** (2010), 186.
3) J. D. Robson and H. K. D. H. Bhadeshia: *Mater. Sci. Technol.*, **13** (1997), 631.
4) F. Abe, V. Taneike and K. Sawada: *Int. J. Press. Vess. Piping*, **84** (2007), 3.
5) K. Maruyama, K. Sawada and J.-I. Koike: *ISIJ Int.*, **41** (2001), 641.
6) K. Yamada, M. Igarashi, S. Muneki and F. Abe: *ISIJ Int.*, **41** (2001), S116.
7) K. Suzuki, S. Kumai, Y. Toda, H. Kushima and K. Kimura: *ISIJ Int.*, **43** (2003), 1089.

8) M. Tamura, Y. Haruguchi, M. Yamashita, Y. Nagaoka, K. Ohinata, K. Ohnishi, E. Itoh, H. Ito, K. Shinozuka and H. Esaka: *ISIJ Int.*, **46** (2006), 1693.
9) A. Yu. Kipelova, A. N. Belyakov, V. N. Skorobogatykh, I. A. Shchenkova and R. O. Kaibyshev: *Metal Sci. Heat Treat.*, **52** (2010), 100.
10) W. B. Jones, C. R. Hills and D. H. Polonis: *Metall. Trans.*, **22A** (1991), 1049.
11) R. C. Thomson and H. K. D. H. Bhadeshia: *Metall. Trans.*, **23A** (1992), 1171.
12) J. M. Vitek and R. L. Klueh: *Metall. Trans.*, **14A** (1983), 1047.
13) S. Kobayashi, K. Toshimori, K. Nakai, Y. Ohmori, H. Asahi and T. Muraki: *ISIJ Int.*, **42** (2002), S72.
14) M. Taneike, K. Sawada and F. Abe: *Metall. Mater. Trans.*, **35A** (2004), 1255.
15) M. Tamura, M. Nakamura, K. Shinozuka and H. Esaka: *Metall. Mater. Trans.*, **39A** (2008), 1060.
16) K. Sawada, K. Kubo and F. Abe: *Mater. Sci. Technol.*, **19** (2003), 732.
17) H. D. Kim and I. S. Kim: *ISIJ Int.*, **34** (1994), 198.
18) A. Yu. Kipelova, A. N. Belyakov, V. N. Skorobogatykh, I. A. Shchenkova and R. O. Kaibyshev: *Metal Sci. Heat Treat.*, **52** (2010), 118.
19) H. Kitahara, R. Ueji, N. Tsuji and Y. Minamino: *Acta Mater.*, **54** (2006), 1279.
20) T. Horiuchi, M. Igarashi and F. Abe: *ISIJ Int.*, **42** (2002), S67.
21) F. Abe, T. Horiuchi and K. Sawada: *Mater. Sci. Forum*, **426** (2003), 1393.
22) M. Tabuchi, M. Kondo, K. Kubo and S. K. Albert: *OMMI*, **3** (2004), 1.
23) S. K. Albert, M. Kondo, M. Tabuchi, F. Yin, K. Sawada and F. Abe: *Metall. And Mater. Trans. A*, **36A** (2005), 333.
24) P. Hofer, M. K. Miller, S. S. Babui, S. A. Davidi and H. Cerjak: *ISIJ Int.*, **42** (2002), S62.
25) H. C. Furtado, L. H. de Almeida and I. Le May: *Mater. Char.*, **58** (2007), 72.
26) G. Dimmler, P. Weinert, E. Kozeschnik and H. Cerjak: *Mater. Char.*, **51** (2003), 341.
27) A. Kipelova, R. Kaibyshev, A. Belyakov and D. Molodov: *Mater. Sci. Eng. A*, **528** (2011), 1280.
28) T. Maki and I. Tamura: *Tetsu-to-Hagané*, **67** (1981), 852.